


 Cite this: *RSC Adv.*, 2022, **12**, 365

Germanium-based superatom clusters as excess electron compounds with significant static and dynamic NLO response; a DFT study†

 Atazaz Ahsin, Ahmed Bilal Shah  and Khurshid Ayub *

Herein, the geometric, electronic, and nonlinear optical properties of excess electron zintl clusters Ge_5AM_3 , Ge_9AM_5 , and $\text{Ge}_{10}\text{AM}_3$ ($\text{AM} = \text{Li}$, Na , and K) are investigated. The clusters under consideration demonstrate considerable electronic stability as well as superalkali characteristics. The NBO charge is transferred from the alkali metal to the Ge-atoms. The FMO analysis shows fabulous conductive properties with a significant reduction in SOMO–LUMO gaps (0.79–4.04 eV) as compared with undoped systems. The designed clusters are completely transparent in the deep UV-region and show absorption in the visible and near-IR region. Being excess electron compounds these clusters exhibit remarkable hyperpolarizability response up to 8.99×10^{-26} esu, where a static second hyperpolarizability (γ_0) value of up to 2.15×10^{-30} esu was recorded for Ge_9Na_5 superatom clusters. The excitation energy is the main controlling factor for hyperpolarizability as revealed from the two-level model study. The electro-optical Pockel's effect and the second harmonic generation phenomenon (SHG) are used to investigate dynamic nonlinear optical features. At a lower applied frequency ($=532$ nm), the dynamic hyperpolarizability and second hyperpolarizability values are significantly higher for the studied clusters. Furthermore, for the Ge_9K_5 cluster, the hyper Rayleigh scattering (HRS) increases to 5.03×10^{-26} esu.

 Received 8th November 2021
 Accepted 4th December 2021

 DOI: 10.1039/d1ra08192f
rsc.li/rsc-advances

1 Introduction

The past several decades have witnessed increasing scientific and technology-driven interest in developing nonlinear optical (NLO) materials because of their tremendous importance in photonic applications.^{1,2} The developments in the field of nonlinear optics and laser-based technologies started after the discovery of the ruby laser by Maiman in 1960.³ Thus nonlinear optical materials have emerged rapidly during the last few decades, mainly due to their extensive applications in optoelectronic and photonic devices, second harmonic generation (SHG), endoscopy, and laser surgery^{4–8} To date, numerous approaches for designing nonlinear optical materials with high hyperpolarizability have been used, including diradical character,⁹ designing octupolar molecules,¹⁰ the push–pull effect in conjugated chromophores,¹¹ multidecker sandwich complexes,¹² and excess electron models.¹³ Among the studied nonlinear optical materials inorganic materials exhibit prime interest because of their physicochemical stability and thermal stability.¹⁴

The excess electron system is well-known for triggering second and third-order nonlinearity.^{15,16} In the family of excess

electron compounds, electride,¹⁷ alkalides,¹⁸ and alkaline-earthides^{19,20} are well known.

Electrides are compounds in which electron trapping into the complexant acts as an anion.²¹ Similarly, the alkalides are compounds in which alkali metals possess a negative charge and become anion (Li^- , Na^- , K^-).²² Alkaline-earthides are also a fabulous excess electron system that contains a negative charge on alkaline-earth metals (Be^- , Mg^- , Ca^-).²³ Excess electron compounds can be designed by doping any complexant with alkali metals,^{24,25} alkaline earth metals,²⁶ transition metals^{27,28} and superalkali clusters.^{29,30}

Superalkali clusters belong to the superatom clusters family and exhibit alkali-like characteristics with tunability in their electronic and geometric properties.³¹ The term 'superalkalis' was first time introduced by Gutsev and Boldyrev for Li_3O , Li_2F , NLi_4 etc. through $\text{DVM}\alpha$ calculations. The superalkali clusters materials are of prime interest and show significant applications in numerous fields including, catalysis,³² reduction of CO_2 and N_2 ,³³ hydrogen storage materials, and nonlinear optics.³⁴ Thus, being excess electron compounds superalkali clusters can be adopted for making high-performance nonlinear optical materials. Furthermore, several studies have been proposed that reveal that superalkali being excess electron clusters can be doped with different molecules and nanocages to form excess electron compounds for triggering the NLO response. In this regard, superalkali-doped nanocages $\text{Li}_3\text{O}@\text{Al}_{12}\text{N}_{12}$ were theoretically designed with electride characteristics for enhanced

Department of Chemistry, COMSATS University Islamabad, Abbottabad Campus, Abbottabad, KPK, 22060, Pakistan. E-mail: khurshid@cuiatd.edu.pk

† Electronic supplementary information (ESI) available. See DOI: [10.1039/d1ra08192f](https://doi.org/10.1039/d1ra08192f)



nonlinear optical response.³⁵ Similarly, superalkali doped 2D graphdiyne M₂X@GDY (where M = Li, Na, K, and X = F, Cl, Br) were studied, and it was observed that there is a significant decrease in the HOMO–LUMO gap with a noticeable increase in hyperpolarizability response.³⁶ Moreover, superalkali clusters were doped with different 2D materials and nanocages to get excess electron compounds *i.e.* alkalide, alkaline earthides. These excess electron compounds were reported as excellent nonlinear optical materials with significant hyperpolarizability.^{24,37,38} However, a very limited number of studies were reported that reveal the nonlinear optical response of pure superalkali clusters as efficient nonlinear optical materials.

A few number of pure superalkali clusters are investigated as excess electron compounds and show remarkable hyperpolarizability. In this regard, Misra *et al.*, investigated the electronic and nonlinear optical response of hyper lithiated superalkali clusters and reported these clusters as efficient NLO materials. The nonlinear optical response increases up to 1.2×10^4 au.³⁹ Subsequently, another class of superalkali clusters CNLi_n ($n = 1-10$) was investigated for nonlinear optical response and second-order NLO response was much pronounced.⁴⁰ The literature reveals that only conventional types of superalkali clusters are explored for optical and nonlinear optical studies however several models can be efficiently utilized to be used as nonlinear optical responses. Literature also reveals, there are several superatom clusters (silicon-based) encapsulated by transition metals which were also studied for optical and magnetic excitation^{41,42}

Zintl polyanions, discovered by Eduard zintl in 1930 belong to the group (14,15) and show excellent physicochemical stability.⁴³ It is previously reported that zintl P₇³⁻ anion as core material can be used to design organo-zintl superalkali clusters which contain superb electron properties.⁴⁴ Similarly, zintl based superalkalis as a building block, when treated with superhalogens make novel supersalt compounds with significant electronic and nonlinear optical properties.⁴⁵ Moreover, superalkali clusters other than alkali metals might possess better stability and a high nonlinear optical response. We became interested in zintl-based superatoms, particularly germinum-based superatoms (which belong to group 14 elements) for electronic and optical properties. Furthermore, the stoichiometry of these clusters obeys magic number nuclei, in which their valence shells are organised as 1S₂, 1P₆, 1D₁₀, 2S₂, 1F₁₄ after losing one electron, achieving electronic shell closure (according to Jellium model). When designed with alkali metals, Ge semimetallic clusters may have improved optoelectronic and NLO features. Although the Ge₅Li₃, Ge₉Li₅, and Ge₁₀Li₃ were theoretically studied by Sun *et al.*⁴⁶ Their investigations were limited to electronic properties whereas we adopted the alkali decorated zintl clusters Ge₅AM₃, Ge₉AM₅ and Ge₁₀AM₅ (where AM = Li, Na, K) for exploring optoelectronic and nonlinear optical properties.

In these studied clusters, we are mainly concerned with the following issues. Do these clusters belong to superalkali with better thermal and electronic stability than conventional superalkalis do these clusters possess nonlinear optical responses for declaring them as efficient NLO materials. The NLO response was confirmed by hyperpolarizability calculation and second hyperpolarizability.

2 Computational details

Initially, all the studied alkali decorated zintl polyanions Ge₅AM₃, Ge₉AM₅, and Ge₁₀AM₃ (where AM = Li, Na, K) are considered and optimized at CAM-B3LYP/6-311+G(d,p) level of theory. The geometries of Ge₅Li₃, Ge₉Li₅, and Ge₁₀Li₃ were reported in the previous literature and we adopted the similar design for the rest of the alkali metals.⁴⁶ All the calculations were performed with Gaussian 09 software.⁴⁷ The CAM-B3LYP (Coulomb attenuating method) is a hybrid exchange–correlation functional that includes the hybrid properties of B3LYP functional and long-range corrected Coulomb-Attenuating Method (CAM).⁴⁸ B3LYP is a hybrid part of the above method that contains Becke 3-parameters for exchange functional and Lee–Yang–Parr-correlation functional. This hybrid density functional theory-based method comprises 0.19 HF plus 0.81 (B88) exchange interactions at short range and 0.65 HF plus 0.35 (B88) long-range interactions.⁴⁹ The CAM-B3LYP is a well-known approach for linear and nonlinear optical characteristics of various clustered materials, and it has already been demonstrated to give appropriate geometries and comparable hyperpolarizability values with CCDST.⁵⁰⁻⁵³ Besides, the triple zeta split valence basis set 6-311+G(d,p) with diffuse and polarized function is adopted throughout the calculations.

To explore the electronic stabilities of these clusters, we calculated vertical ionization potential and electron affinity.

$$\text{IE} = E_{\text{X}}^+ - E_{\text{X}}^0 \quad (1)$$

$$\text{EA} = E_{\text{X}}^- - E_{\text{X}}^0 \quad (2)$$

The chemical hardness is also calculated to understand their reactivity and soft nature and given by equation below⁵⁴

$$\text{Chemical hardness} (\eta) = \text{VIP} - \text{VEA} \quad (3)$$

To further explore the electronic properties, we performed frontier molecular orbital (FMOs) analysis which included SOMO, LUMO, and $E_{\text{H-L}}$ gap. The FMOs analysis also provides evidence of the excess electron nature of studied superalkali clusters. Natural bonding orbital (NBO) study is conducted to explore the nature and charge distribution as studied superatom clusters. The time-dependent density functional (TD-DFT) theory is adopted to calculate the excited state parameters and absorbance behavior of studied zintl superatom clusters. The time-dependent density functional (TD-DFT) is well known for obtaining excited states parameters and absorption spectra of molecules and clusters. The TD-DFT was chosen because of its performance and its correspondence to experimental results. For this purpose excited-state calculations with TD-CAM-B3LYP/6-311+G(d,p) are performed. Mathematically system under the constant field can be expressed as:

$$E(F) = E^0 - \mu_i F_i - \frac{1}{2} \alpha_{ij} F_i F_j - \frac{1}{6} \beta_{ijk} F_i F_j F_k - \frac{1}{24} \gamma_{ijkl} F_i F_j F_k F_l \dots \quad (4)$$



where F is an external applied electric field on the molecular system, F_i is its component of force along i direction; E^0 is the total energy of the superalkali clusters without a static electric field, μ_i , α_{ij} , β_{ijk} , and γ_{ijkl} are dipole moment, polarizability, hyperpolarizability, and second-order hyperpolarizability, respectively. Thus regarding nonlinear optical properties, the following parameters are estimated including the mean dipole moment (μ_o), change in dipole moment ($\Delta\mu$), static polarizability (α) and static first hyperpolarizability (β).

$$\alpha_o = 1/3(\alpha_{xx} + \alpha_{yy} + \alpha_{zz}) \quad (5)$$

$$\beta_0 = \sqrt{\beta_x^2 + \beta_y^2 + \beta_z^2} \quad (6)$$

where $\beta_x = \beta_{xxx} + \beta_{xyy} + \beta_{xzz}$, $\beta_y = \beta_{yyy} + \beta_{yzz} + \beta_{yxx}$ and $\beta_z = \beta_{zzz} + \beta_{zxx} + \beta_{zyy}$.

$$\mu_o = (\mu_x^2 + \mu_y^2 + \mu_z^2)^{1/2} \quad (7)$$

Besides, the second static hyperpolarizability (γ_o) and the projection of hyperpolarizability on the dipole moment vector (β_{vec}) is also calculated for our studied superalkali clusters at the same level of theory. Vector part of hyperpolarizability (β_{vec}) and second hyperpolarizability (γ) are expressed defined as

$$\langle \gamma \rangle = 1/5(\gamma_{xxxx} + \gamma_{yyyy} + \gamma_{zzzz} + \gamma_{xxyy} + \gamma_{xxzz} + \gamma_{yyxx} + \gamma_{yyzz} + \gamma_{zzxx}) \quad (8)$$

$$\beta_{vec} = \sum \frac{\mu_i \beta_i}{|\mu|} \quad (9)$$

Mathematically β_{HRS} can be expressed as;

$$\beta_{HRS}(-2\omega; \omega, \omega) = \sqrt{\langle \beta_{zzz}^2 \rangle + \langle \beta_{zxx}^2 \rangle} \quad (10)$$

where $\langle \beta_{zzz}^2 \rangle$ and $\langle \beta_{zxx}^2 \rangle$ are average of orientational (β) tensor.

While the related depolarization ratio for these superalkali clusters (DR) ratio is also given by;

$$DR = \langle \beta_{zzz}^2 \rangle / \langle \beta_{zxx}^2 \rangle$$

The frequency-dependent NLO analysis was conducted at 532 and 1064 nm wavelength. Frequency-dependent hyperpolarizability involves the electro-optic Pockel's effect (EOPE) $\beta(-\omega; \omega, 0)$ and electric field induced second harmonic generation (ESHG) $\beta(-2\omega; \omega, \omega)$ respectively. While for second hyperpolarizability (γ), dc-Kerr $\gamma^{dc\text{-Kerr}}(\omega) = \gamma(-\omega; \omega, 0, 0)$ and second harmonic generation $\gamma^{ESHG}(\omega) = \gamma(-2\omega; \omega, \omega, 0)$ were considered.

3 Results and discussion

3.1 Geometries and electronic properties

All the optimized geometries of Ge_5AM_3 , Ge_9AM_5 , and $Ge_{10}AM_3$ (where $AM = Li, Na, K$) zintl superalkali clusters and their equilibrium bond length are depicted in Fig. 1. The geometric

parameters of these clusters are identical to those reported in the earlier literature⁴⁶ and are included in the ESI† (S1).

These clusters have no imaginary frequency (negative frequency) according to the frequency calculations, hence they are true minima on the potential energy surface (PES).

The computed ionization potential and electron affinity are used to analyze the electronic stability and superalkali nature of the investigated clusters. The difference in ground state energy between the cationic and neutral systems is described as the ionization potential (IP), meanwhile, the difference in ground state energy between the neutral and anionic systems is defined as the electron affinity.

The vertical ionization potential (VIP) values for Ge_9AM_3 are in the range of 5.49 to 3.91 eV, and it decreased dramatically as the alkali-metal size rose (Li to k). The VIP values for the Ge_9AM_5 series follow a similar pattern, reaching to 2.15 eV for F (Table 1). On the other hand, the VIP values for $Ge_{10}AM_3$ are slightly higher than for Ge_9AM_5 (Table 1). The lower VIPS values for the Ge_9AM_5 series can be attributed to the higher number of alkali metals ($AM = 5$), which is responsible for the cluster's electro-positive nature. Additionally, their superalkali nature is demonstrated by their relatively low ionization potential values than Li atoms (5.4 eV).

The calculated vertical electron affinity (VEA) values of these superalkali clusters range from 0.02 to 1.15 eV. In the designed series, Ge_9AM_5 has a smaller VEA value than those of Ge_3AM_3 and $Ge_{10}AM_3$. The electro-positive feature of the examined superalkalis is revealed by the tiny VEA values. Furthermore, the reduced VEA values indicate that these alkali-decorated zintl clusters are unable to completely grasp the valence (loosely bound) electron, which could result in interesting electrical properties. Table 1 shows that the examined clusters are polarizable and soft, based on the computed minimal values of chemical hardness. The calculated chemical hardness (η) values decrease with increased alkali metals size within these clusters. Among the series, Ge_9AM_5 clusters shows lower values of chemical hardness which may be attributed to the higher number of alkali smaller metals (soft) in these clusters.

3.2 Natural bonding orbital (NBO) analysis

The NBO analysis is a useful tool for interpreting intramolecular and intermolecular interactions and conjugative interactions in compounds and clusters.⁵⁵ For Ge_5AM_3 clusters, the obtained charges on alkali metals (QAM) vary from 0.86 to 0.90|e| (positive magnitude). The C cluster has the highest computed positive charge of 0.90|e|, while A has the lowest value of 0.86|e| in the Ge_5AM_3 family. Similarly, the Ge_9AM_5 clusters, computed average charge (QAM) ranges from 0.85 to 0.90|e| (Table 1). For the $Ge_{10}AM_3$ superalkali clusters, similar NBO (positive magnitude) charges are observed. Hence, the computed positive NBO charges upon alkali metals shows the significant charge transfer (from alkali metals to Ge-atom) within the superalkali clusters. Additionally, the computed NBO charges upon germanium metals (Q_{Ge}) for Ge_5AM_3 range from -0.13 to -0.69|e| (negative in magnitude). Therefore from the computed NBO charges (Table 1) one can observe the excellent separation of



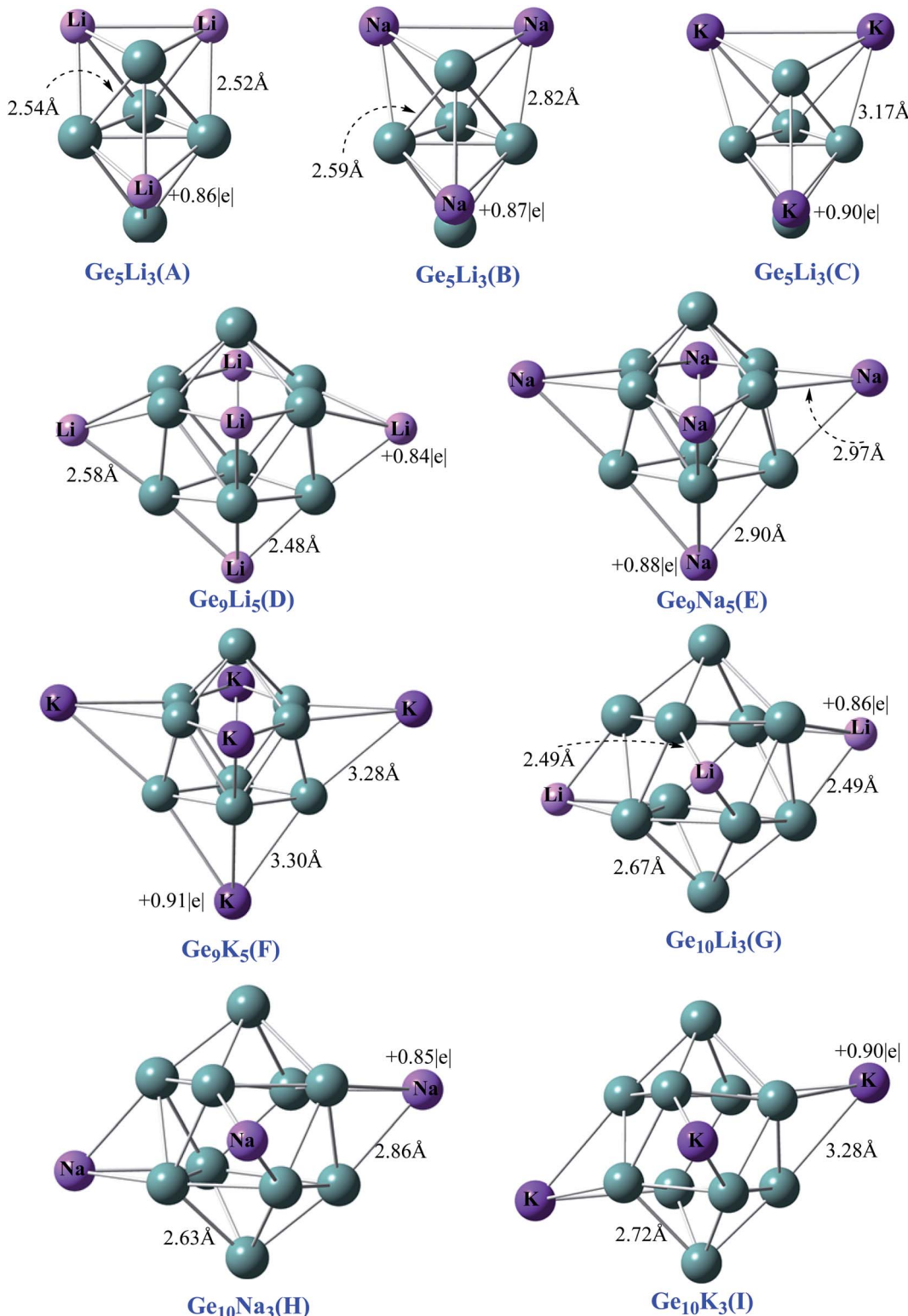


Fig. 1 Optimized geometries with NBO charge of Ge_5AM_3 , Ge_9AM_5 and $\text{Ge}_{10}\text{AM}_3$ clusters.

charges within the clusters. Likewise, the computed NBO charges (Q_{Ge}) for the Ge_9AM_3 clusters are range from -0.09 to $-0.61|e|$ where the highest value of $-0.61|e|$ is obtained for Ge_9Li_5 while the lowest value (-0.50) is obtained for Ge_9K_5

superalkali. However, the reported NBO charges (Q_{Ge}) for the third series $\text{Ge}_{10}\text{AM}_3$ are reduced (in negative magnitude) with corresponding increased cluster size. The overall NBO charges is an order of $\text{Ge}_5\text{AM}_3 > \text{Ge}_9\text{AM}_5 > \text{Ge}_{10}\text{AM}_3$.



Table 1 Vertical ionization potential (VIP, in eV), vertical electron affinity (VEA in eV), maximum chemical hardness (η in eV), average NBO charge upon germanium (Q_{Ge} in $|\text{e}|$), an average charge upon alkali metal (Q_{AM} in $|\text{e}|$), of Ge_5AM_3 Ge_9AM_5 and $\text{Ge}_{10}\text{AM}_3$ (where AM = Li, Na, K)

Superalkalis	VIP	VEA	η	Q_{Ge}	Q_{AM}
Ge_5AM_3 (where AM = Li, Na, K)					
Ge_5Li_3 (A)	5.49	0.98	4.51	-0.69	0.86
Ge_5Na_3 (B)	4.69	0.64	4.05	-0.65	0.87
Ge_5K_3 (C)	3.91	0.29	3.62	-0.65	0.90
Ge_9AM_5					
Ge_9Li_5 (D)	4.36	0.65	3.71	-0.61	0.85
Ge_9Na_5 (E)	2.81	0.07	2.74	-0.52	0.88
Ge_9K_5 (F)	2.15	0.02	2.13	-0.50	0.90
$\text{Ge}_{10}\text{AM}_3$					
$\text{Ge}_{10}\text{Li}_3$ (G)	4.98	1.15	3.83	-0.38	0.86
$\text{Ge}_{10}\text{Na}_3$ (H)	4.34	0.67	3.67	-0.36	0.85
Ge_{10}K_3 (I)	3.50	0.11	3.39	-0.46	0.90

3.3 Frontier molecular orbital (FMO) analysis and excess electron character

FMO analysis is adopted to validate the reactivity of the studied cluster system. Thus according to the frontier molecular orbital treatment of chemical reactivity, the rate, and site of reactivity of a molecule with a nucleophile is dominated by the interaction of the LUMO of the molecule in question with the HOMO of the nucleophile. The closer these orbitals are in energy, the more intensely they will interact, and the higher is the reactivity will be. Result in Table 2 show that the computed values for singly occupied molecular orbitals (SOMO), LUMO, and $E_{\text{S-L}}$ gaps. For the Ge_5AM_3 , the obtained values of singly occupied molecular orbitals (SOMO) vary from -4.99 to -3.51 eV and increase from A to C. For Ge_9AM_5 , predicted SOMO energies are in the range of -3.97 to -1.80 eV, as well. The $\text{Ge}_{10}\text{AM}_3$ clusters, on the other hand, have lower SOMO energies than those of Ge_9AM_5 clusters, and these range from -4.46 to -3.14 eV. It can also be concluded that the SOMO energies of the examined superalkali clusters rise monotonically as the size of the alkali metals increases. Thus the observed trend of SOMO energies for studied superalkali clusters is $\text{Ge}_9\text{AM}_5 < \text{Ge}_{10}\text{AM}_3 < \text{Ge}_5\text{AM}_3$. Furthermore, the estimated LUMO energies for Ge_5AM_3 clusters vary with cluster size. However, the estimated energies of virtual orbitals for the Ge_9AM_5 series are increasing, while the $\text{Ge}_{10}\text{AM}_3$ clusters are increasing even high.

For Ge_5AM_3 clusters, there is a considerable reduction in the SOMO–LUMO gap, with values ranging from 4.06 to 2.77 eV. The HOMO–LUMO gaps for Ge_5AM_3 clusters are around 4.06 to 2.77 eV, indicating that these compounds behave like semiconductors. Similarly, the observed reduction in Ge_9AM_5 $E_{\text{H-L}}$ values from 3.89 to 0.79 eV could be attributable to their higher SOMO energies. Furthermore, the $\text{Ge}_{10}\text{AM}_3$ series' HOMO–LUMO gap values are slightly higher than the Ge_9AM_5 series, and range from 3.37 to 2.45 eV (Table 2). The significant reduction in HOMO–LUMO gaps reveals the soft nature (higher reactivity) and conductive properties of these clusters.

Table 2 Energies of SOMO and LUMOs (in eV), HOMO–LUMO gaps ($E_{\text{H-L}}$ in eV), excitation energies (ΔE in eV), the wavelength of maximum absorbance (λ_{max} in nm), oscillator strength (f_o in au), ground-state dipole moment (μ_o in au), and excited-state dipole moment ($\Delta\mu$ in au) of Ge_5AM_3 , Ge_9AM_5 and $\text{Ge}_{10}\text{AM}_3$ superalkali clusters

Superalkalis	SOMO	LUMO	$E_{\text{H-L}}$	ΔE	λ_{max}	f_o	μ	$\Delta\mu$
Ge_5AM_3 (where AM = Li, Na, K)								
Ge_5Li_3 (A)	-4.99	-0.94	4.04	2.16	571	0.015	1.63	1.05
Ge_5Na_3 (B)	-4.24	-0.99	3.25	2.16	572	0.015	2.26	1.14
Ge_5K_3 (C)	-3.51	-0.73	2.77	2.24	553	0.041	3.12	2.34
Ge_9AM_5								
Ge_9Li_5 (D)	-3.97	-0.07	3.89	2.25	548	0.007	0.27	0.62
Ge_9Na_5 (E)	-2.42	-1.07	1.34	1.77	688	0.076	1.69	2.49
Ge_9K_5 (F)	-1.80	-1.02	0.79	1.12	1101	0.219	2.21	1.86
$\text{Ge}_{10}\text{AM}_3$								
$\text{Ge}_{10}\text{Li}_3$ (G)	-4.40	-0.87	3.73	2.31	534	0.007	1.45	0.62
$\text{Ge}_{10}\text{Na}_3$ (H)	-4.00	-0.83	3.16	2.47	500	0.008	1.55	0.65
Ge_{10}K_3 (I)	-3.14	-0.69	2.45	2.14	578	0.005	1.67	0.49

Furthermore, the observed reduced SOMO–LUMO gap within clusters is attributed to the larger size of alkali metals (ease in the transition of electron from occupied to virtual orbitals).

Moreover, the excess electron character of clusters can be seen in the electronic density distribution (Fig. 2). The excess electron cloud is indicated by the electronic density of SOMO and LUMO scattered throughout the alkali metals that resemble to s-orbital. The LUMO electronic density for $\text{Ge}_{10}\text{AM}_3$ clusters wraps around the alkali metals, whereas the LUMO densities for Ge_9AM_5 clusters move away from the alkali metals.

3.4 TD-DFT analysis of clusters

Time-dependent density functional theory was used to examine the absorbance behavior of Ge_5AM_3 , Ge_9AM_5 , and $\text{Ge}_{10}\text{AM}_3$ superalkali clusters. For nonlinear optical applications, the cluster materials employed should be transparent in the used region. In the absorption study, we calculated the maximum absorbance, excitation energy, and oscillator strength (during the electronic transition). The computed excited state parameters for the studied superalkali clusters are given in Table 2. From the computed results one can observe that the studied clusters are completely transparent in the UV-region (<400 nm) and show broadband absorbance in the visible region. The longer absorbance wavelength for the Ge_5AM_3 ($\lambda_{\text{max}} = 572$ nm) is observed for the Ge_5Na_3 superalkali cluster whereas the lowest absorbance maxima ($\lambda_{\text{max}} = 553$ nm) is obtained for the Ge_5K_3 superalkali cluster (Fig. 3). However, the Ge_9AM_5 series shows higher absorbance maxima ($\lambda_{\text{max}} = 1101$ nm) for Ge_9K_5 clusters. Similarly, for the second series, the highest absorbance maxima ($\lambda_{\text{max}} = 578$ nm) is observed for the Ge_{10}K_3 cluster in the $\text{Ge}_{10}\text{AM}_3$ series. Overall, the clusters of Ge_9AM_5 series shows absorption maxima at a longer wavelength (bathochromic shift) whereas the Ge_5AM_3 and $\text{Ge}_{10}\text{AM}_3$ have slightly blue-shifted wavelengths. As a result of their total transparency under deep UV-region, the optoelectronic properties of the examined



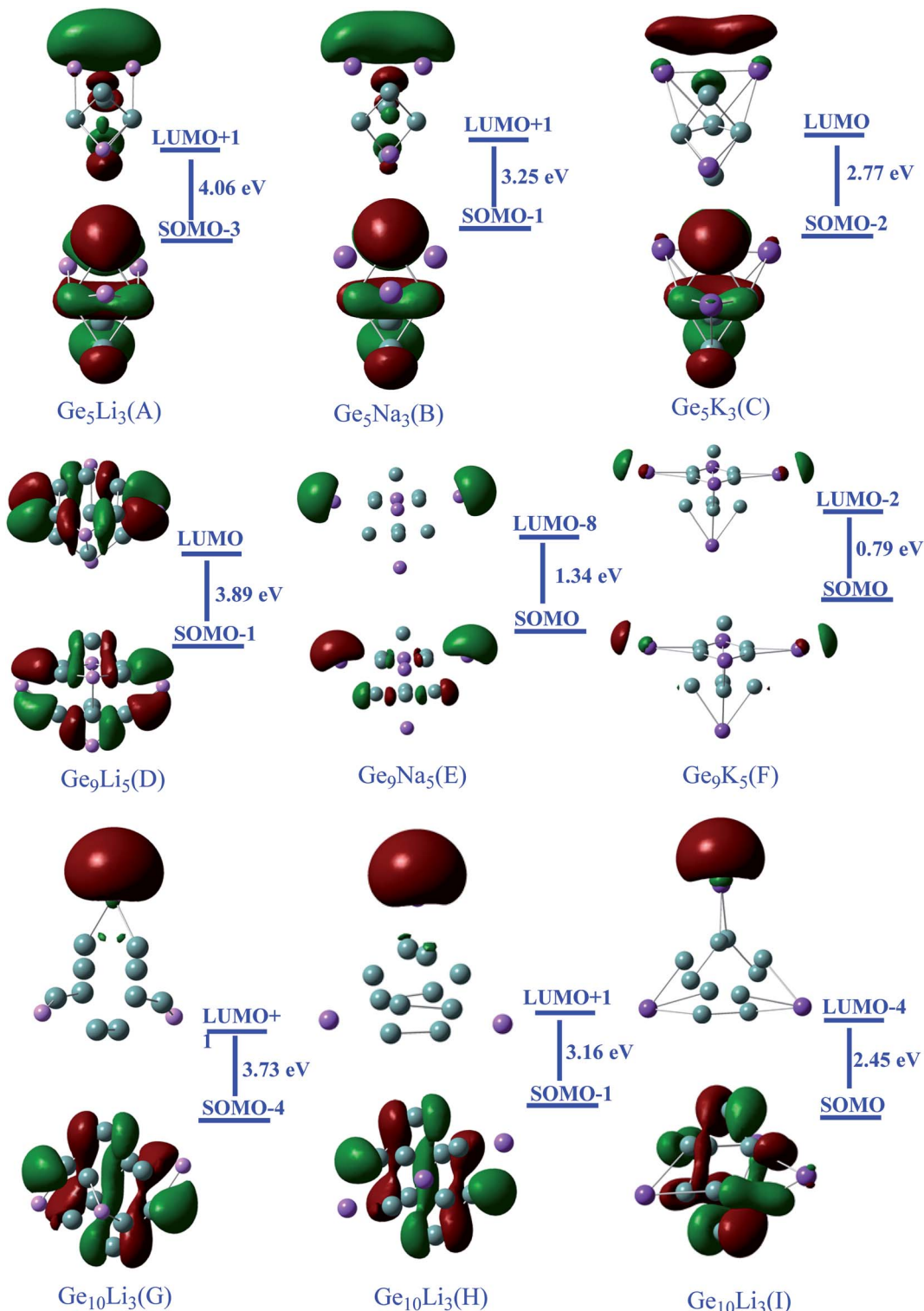


Fig. 2 Representation of Frontier molecular orbital densities along with orbitals contribution of superalkali clusters (iso-value of 0.030).

clusters fall under the UV-region. Furthermore, the excitation energies (ΔE) of Ge_5AM_3 (*i.e.* excitation of an electron from HOMO to LUMO) are also very small and ranges from 2.16 to 2.24 eV whereas the observed excitation energies (ΔE) for the Ge_9AM_5 are further reduced and lie in the range of 1.12 to

2.25 eV. Alternatively, the computed excitation energies of the $\text{Ge}_{10}\text{AM}_3$ series are slightly higher than those of Ge_9AM_5 and display a range of 2.14 to 2.47 eV. Moreover, the calculated oscillator strength (probability of absorbance during excitation) shows significant values for Ge_5AM_3 superalkali clusters while



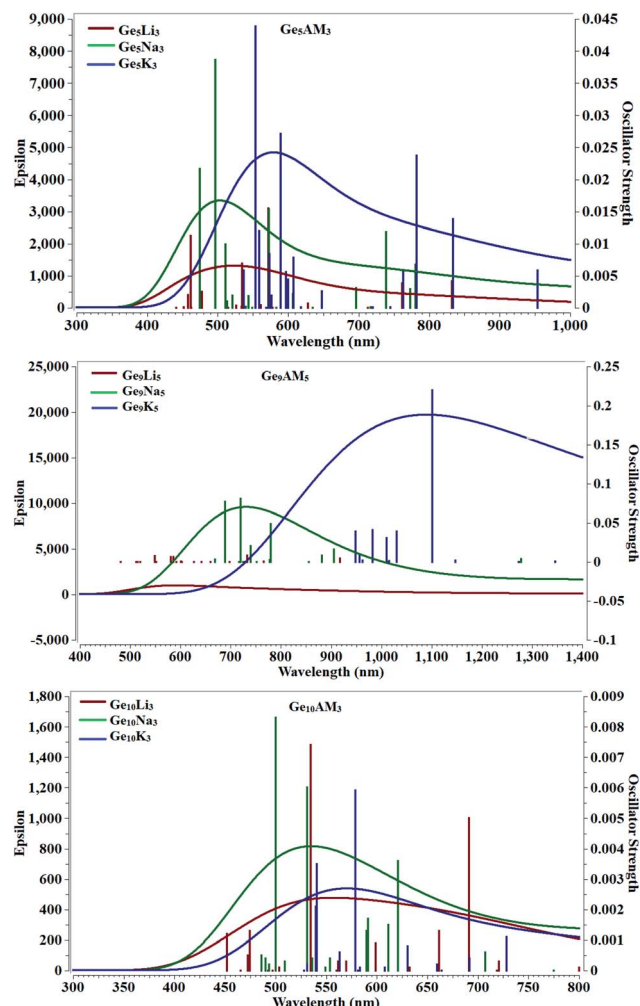


Fig. 3 Absorbance spectra of Ge_5AM_3 , Ge_9AM_5 , and $\text{Ge}_{10}\text{AM}_3$.

the Ge_9AM_5 and $\text{Ge}_{10}\text{AM}_3$ have slightly reduced values of oscillator strength (f_0).

3.5 Dipole moment and change in dipole moment

Table 2 shows the computed values of mean dipole moment (μ_0) and change in dipole moment ($\Delta\mu$). The magnitude of polarisation in clusters and the asymmetric charge distribution are shown by the significant values of dipole moments. For the Ge_5AM_3 series, the observed mean dipole moments range from 1.63 to 3.13 au. As the size of alkali metals grows larger (Li to K), the dipole moment gradually increase. Likewise, the calculated values of the dipole moment of Ge_9AM_5 range from 0.27 to 2.21 au. Thus the calculated values of dipole moment for the Ge_9AM_5 are slightly smaller than those of Ge_5AM_3 clusters. On the other hand, the computed mean dipole moments are enhanced for the $\text{Ge}_{10}\text{AM}_3$ series and the values lie in the range of 1.42 to 1.67 au. Hence, from the computed results, one can conclude that a significant dipole moment that is associated with the Ge_5AM_3 series would result in larger polarization. Our calculations also show that the studied alkali decorated zintl polyanions clusters possess polar bonds (asymmetric electronic density) that might

be an important factor for imparting optical and nonlinear optical properties. Besides, the computed changes in dipole moment between the ground state and crucial excited state for Ge_5AM_3 clusters lies in the range of 1.05 to 2.34 au where the highest value of 2.34 au is observed for Ge_5K_3 while the lowest value of 1.05 au is obtained for the Ge_5Li_3 cluster. A similar decreasing trend of change in dipole moment is observed for the Ge_9AM_5 clusters. The value of excited-state dipole moment for the Ge_9AM_5 series lie in the range of 0.62 to 1.86 au. However, the computed values of the excited-state dipole moment are increasing with the increased size of alkali metals within clusters. Finally, the $\text{Ge}_{10}\text{AM}_3$ series of clusters show further decreased values of change in dipole moment. As a result of the fascinating electronic features of clusters examined, increased optical and nonlinear optical properties might be expected.

3.6 Static nonlinear optical properties

The alkali-like superatom clusters Ge_5AM_3 , Ge_9AM_5 , and $\text{Ge}_{10}\text{AM}_3$ examined here have an excess electron nature. As a result, large optical and nonlinear optical (NLO) responses are reasonable predictions. Literature reveals that compounds and clusters with excess electrons characteristics are significantly adopted for triggering nonlinear optical response.^{19,36,39,56-65} Hence, the calculated polarizability (α_0), hyperpolarizability (β_0), second hyperpolarizability (γ_0), and associated electronic parameters are computed and given in Table 3. The calculated values of polarizability (linear optical response) of Ge_5AM_3 lie in the range of 3.70×10^{-23} to 5.3×10^{-23} esu. Similarly, the computed values of polarizability (α_0) for Ge_9AM_5 series are significantly enhanced and lie in the range of 6.5×10^{-23} to 1.9×10^{-21} esu. Alternatively, the obtained values of polarizability of $\text{Ge}_{10}\text{AM}_3$ series are slightly smaller than those of Ge_9AM_5 and lie in range of 60×10^{-24} to 71×10^{-24} au. The increasing trend of polarizability may be seen as the size of alkali metals increases (Li to K). Overall, the highest value of 1.9×10^{-21} esu is obtained for F wheres the lowest value of 37×10^{-24} esu is observed for A. Furthermore, the significant polarizability values obtained demonstrate the amount of polarity within the examined clusters. Asymmetric distribution of charges and electronic densities inside clusters also contributed to the higher linear optical response.

Furthermore, the calculated values of static hyperpolarizability (β_0) lie in the range of 3.44×10^{-29} to 8.99×10^{-26} esu. The calculated static first and second hyperpolarizabilities values are significant. Hyperpolarizability values in the proposed superalkali clusters follow the order $\text{Ge}_9\text{AM}_5 > \text{Ge}_5\text{AM}_3 > \text{Ge}_{10}\text{AM}_3$. The hyperpolarizability values obtained for the Ge_5M_3 series rise monotonically with alkali metal size. The highest value of 3.41×10^{-28} esu is observed for the C cluster while the lowest value (3.44×10^{-29} esu) is calculated for the A cluster. Similarly, the obtained values of the β_0 for the Ge_9AM_5 series range from 1.80×10^{-28} to 8.99×10^{-26} esu. With the increased metal size and the number of alkali metals in the Ge_9AM_5 clusters, there is a huge increase in β_0 values. In particular, the Ge_9K_3 shows a remarkable β_0 value (8.99×10^{-26}



Table 3 Polarizability (α_o in $\times 10^{-24}$ esu), first static hyperpolarizability (β_o in $\times 10^{-33}$ esu) scattering hyperpolarizability (β_{vec} in $\times 10^{-33}$ esu), static second hyperpolarizability (γ_o in $\times 10^{-40}$ esu), HOMO–LUMO gaps (E_{H-L} in au), and vertical ionization potential (VIP in au) of Ge_5AM_3 , Ge_9AM_5 and $Ge_{10}AM_3$ superalkali clusters

Superalkalis	α_o	β_o	β_{vec}	γ_o	E_{H-L}	VIP
Ge_5AM_3						
Ge_5Li_3 (A)	3.7×10^{-23}	3.44×10^{-29}	3.39×10^{-30}	1.37×10^{-34}	4.04	5.49
Ge_5Na_3 (B)	4.5×10^{-23}	1.01×10^{-27}	9.94×10^{-30}	5.5×10^{-34}	3.25	4.69
Ge_5K_3 (C)	5.3×10^{-23}	3.41×10^{-28}	2.97×10^{-29}	2.80×10^{-33}	2.77	3.91
Ge_9AM_5						
Ge_9Li_5 (D)	6.5×10^{-23}	1.80×10^{-28}	1.81×10^{-29}	4.07×10^{-34}	3.89	4.36
Ge_9Na_5 (E)	3.6×10^{-22}	1.57×10^{-26}	1.57×10^{-26}	2.15×10^{-30}	1.34	2.81
Ge_9K_5 (F)	1.9×10^{-21}	8.99×10^{-26}	8.99×10^{-27}	7.68×10^{-34}	0.79	2.15
$Ge_{10}AM_3$						
$Ge_{10}Li_3$ (G)	6.0×10^{-23}	1.88×10^{-29}	1.88×10^{-29}	2.26×10^{-34}	3.73	4.98
$Ge_{10}Na_3$ (H)	6.8×10^{-23}	3.87×10^{-29}	3.87×10^{-29}	3.87×10^{-34}	3.16	4.34
$Ge_{10}K_3$ (I)	7.1×10^{-23}	4.57×10^{-29}	4.57×10^{-29}	7.68×10^{-34}	2.45	3.50

esu) which may be attributed to the larger size of alkali metal (K). In comparison, the $Ge_{10}AM_3$ (AM = Li, Na, and K) clusters have range of 1.88×10^{-29} to 4.57×10^{-29} , which is lower than the Ge_9AM_5 and Ge_5AM_3 clusters. In our designed and studied clusters the hyperpolarizability response is quite larger than previously reported Li_nF ($n = 2-5$) superalkali clusters,³⁹ and M_2OCN & M_2NCO (M = Li, Na, K) clusters.⁶⁴ Excess electron nature might account for considerable hyperpolarizability response found in these clusters. Furthermore, the studied fabulous electronic properties contribute to the hyperpolarizabilities values. As a result, decreased E_{H-L} gaps and ionization potential (IP) with increasing alkali metals (AM) size ultimately prompt the β_o response.

We used a conventional two model with the sum-over-state (SOS) method to develop a full understanding of hyperpolarizability and its governing factors. The two-level model can be written as follows: $\beta_{tl} = \Delta\mu \times f_o / \Delta E^3$

Where the $\Delta\mu$, f_o , and ΔE are changes in dipole moment, oscillator strength, and excitation energy for crucial excitation (excitation with maximum oscillator strength). From the above model, one can observe that β_{tl} has a direct relation with change in dipole moment and oscillator strength (f_o) while it is inversely related with cubic of excitation energy (ΔE). The obtained values of β_{tl} range from 1.03×10^{-29} – 1.90×10^{-27} esu (Table 4). The Ge_9AM_5 has the largest β_{tl} values in the examined clusters series, which is comparable to β_o . For the first series (Ge_5AM_3), the β_{tl} is increased with an increase in $\Delta\mu$ and oscillator strength. In this series, Ge_5K_3 shows a significant β_{tl} response which may be attributed to its noticeable change in dipole moment (2.34 au) and small excitation energy (1.58 eV). As a result, excitation energy (E) is considered to be extremely vital in impacting hyperpolarizability response. A similar trend is observed for the second series (Ge_9AM_5) where the Ge_9Na_5 shows a notable value (1.90×10^{-27} esu) of β_{tl} which is due to small excitation energy (transition energy) and higher change in dipole moment (2.49 au). Likewise, β_{tl} values for the $Ge_{10}AM_3$ series, there is an increase β_{tl} with reduced excitation energy (ΔE). Hence, the excitation energy is deciding factor in

triggering the hyperpolarizability response from the two-level model where its effect is inversely related to β_{tl} . Furthermore, the estimated β_o and β_{tl} values are highly correlated, providing additional insight into the hyperpolarizability response. From the plotted graph (Fig. 4), one can observe that overall, the β_{tl} values increase dramatically for the Ge_9Na_5 cluster.

Projection of hyperpolarizability on dipole moment vector is also evaluated through β_{vec} simulations. The β_{vec} is a vector part of hyperpolarizability and is very important to characterize the nonlinearity of molecules and clusters. The calculated β_{vec} values are given in Table 3. From Table 3, the observed β_{vec} response of designed clusters strongly correlates with total hyperpolarizability which indicates the dipole moment has the same direction projection of hyperpolarizability (β_o). Furthermore, the quite comparable values of first hyperpolarizabilities with β_{vec} also indicate that the charge transfer is parallel to the

Table 4 Computed hyperpolarizability from the two-level model (β_{tl} in $\times 10^{-33}$ esu), change in dipole moment ($\Delta\mu$ in au), excitation energy (ΔE in eV), oscillator strength (f_o in au) hyper Rayleigh scattering (β_{HRS} in $\times 10^{-33}$ esu), and depolarization ratio (DR in au) of superalkali clusters

Superalkalis	β_{tl}	$\Delta\mu$	ΔE	f_o	β_{HRS}	DR
Ge_5AM_3						
Ge_5Li_3 (A)	1.03×10^{-29}	1.05	2.16	0.05	1.31×10^{-29}	6.87
Ge_5Na_3 (B)	3.11×10^{-29}	1.14	1.67	0.04	4.23×10^{-29}	5.61
Ge_5K_3 (C)	9.79×10^{-29}	2.34	1.58	0.16	1.32×10^{-28}	6.41
Ge_9AM_5						
Ge_9Li_5 (D)	2.90×10^{-30}	0.62	1.69	0.01	1.13×10^{-29}	2.44
Ge_9Na_5 (E)	1.90×10^{-27}	2.49	0.01	0.002	9.61×10^{-27}	2.41
Ge_9K_5 (F)	9.83×10^{-28}	1.86	0.75	0.06	5.03×10^{-26}	2.45
$Ge_{10}AM_3$						
$Ge_{10}Li_3$ (G)	1.54×10^{-30}	0.62	1.87	0.01	1.21×10^{-29}	2.37
$Ge_{10}Na_3$ (H)	1.79×10^{-30}	0.65	2.02	0.21	2.08×10^{-29}	2.45
$Ge_{10}K_3$ (I)	9.64×10^{-31}	0.49	1.86	0.11	2.73×10^{-29}	2.57



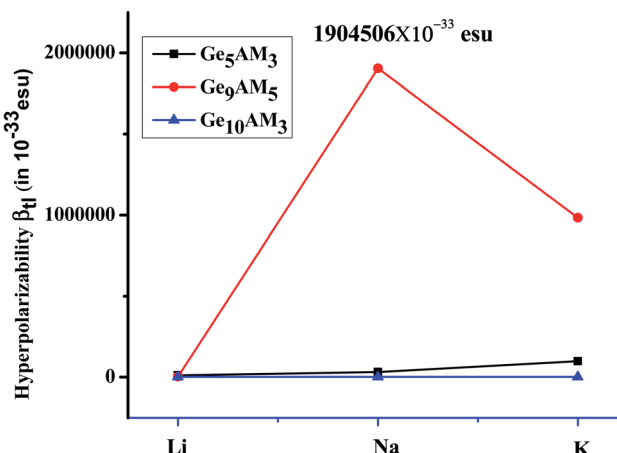


Fig. 4 Representation of β_{tt} for Ge_5AM_3 , Ge_9AM_5 , and $\text{Ge}_{10}\text{AM}_3$ superalkali clusters.

molecular dipole moments. The resemblance of β_o and β_{vec} also suggests that these clusters can be synthesized in laboratory.

We also carried out calculations for estimation of static second hyperpolarizability (γ_o) which is a third rank tensor (χ^3). The obtained values of γ_o for the Ge_5AM_3 range from 1.37×10^{-34} to 2.80×10^{-33} esu which shows an increasing trend with the increased size of alkali metals. Similarly, for the second series (Ge_9AM_5), the γ_o response increases up to 2.15×10^{-30} esu for E cluster. The γ_o values for the $\text{Ge}_{10}\text{AM}_3$ superalkali clusters, on the other hand, decrease considerably. Clusters with a higher number of alkali metals (AM) have a substantial γ_o response. Likewise, the γ_o response for the $\text{Ge}_{10}\text{AM}_3$ clusters lie in the range of 2.26×10^{-34} to 7.68×10^{-34} esu and a slight increase is observed with growing alkali metals size. Hence, the γ_o values vary in order of $\text{Ge}_9\text{AM}_5 > \text{Ge}_5\text{AM}_3 > \text{Ge}_{10}\text{AM}_3$.

3.7 Hyper Rayleigh scattering measurement (β_{HRS})

The hyperpolarizability of nonlinear optical molecules can be determined using hyper-Rayleigh scattering. The β_{HRS} is a widely used method for determining the nonlinear optical characteristics of centrosymmetric molecules with zero dipole moment. At the same level of theory, we theoretically evaluated the β_{HRS} response for these clusters. Overall, the calculated highest value (5.03×10^{-26} esu) of β_{HRS} is obtained for Ge_9K_5 while the lowest value 1.13×10^{-29} esu is observed for D. For the Ge_5AM_3 series β_{HRS} lie in the range of 1.31×10^{-29} esu to 1.32×10^{-28} esu, and are increased with size (Li to K). In the Ge_9AM_5 series, the usual trend of beta-HRS value of Ge_9Li_5 may be attributed to the small size of Li-atom. Similarly, other nonlinear optical parameters for Ge_9Li_5 are also small. It has been reported in the literature previously that dominating factor changes from structure to structure (and it ultimately leads to irregular trends). However, factors affecting the β_{HRS} response might be the same as total hyperpolarizability values. A similar increasing trend of β_{HRS} with the size of metal (AM) can be seen for the second series of clusters (Ge_9AM_5). Furthermore, β_{HRS} values do not increase with clusters size,

rather these show dependence upon the size of and the number of alkali metals. As a result, the β_{HRS} values for the $\text{Ge}_{10}\text{AM}_3$ become slightly smaller, ranging from 1.22×10^{-29} to 2.73×10^{-29} esu. Interestingly, the Ge_9K_5 exhibits a significant HRS response which suggests better NLO properties. Additionally, the depolarization ratio (DR) is higher for Ge_5AM_3 clusters and increases up to 6.87 au for Ge_5Li_3 .

3.7.1 Dynamic nonlinear optical properties. The frequency-dependent NLO properties are the fundamental molecular parameters that are required for the description of many nonlinear optical phenomena. The theoretical understanding and accurate determination of the frequency-dependent hyperpolarizabilities $\beta(\omega)$ and second hyperpolarizabilities $\gamma(\omega)$ are therefore crucial to classify nonlinearity of materials. The frequency-dependent NLO response is estimated at dispersion frequencies of 532 and 1064 nm, and we calculated electro-optic pockel's effect (EOPE) with $\beta(-\omega;\omega,0)$ and electric field induced second harmonic generation (EFSHG) with $\beta(-2\omega;\omega,\omega)$ at applied frequency. The obtained values of electro-optical pockel's effect (EOPE) for Ge_5AM_3 clusters at dispersion frequency of 532 nm range from. The EOPE effect is much pronounced at a small dispersion frequency of 532 nm. Similarly, the obtained dynamic hyperpolarizabilities $\beta(-2\omega;\omega,\omega)$ values noticeably at smaller frequencies. Overall, the highest values (3.54×10^{-26} esu) of EOPE is obtained for C whereas the lowest value of 3.02×10^{-28} esu is observed for D (Table 5). The is a gradual increase in $\beta(\omega)$ with an increased size of alkali metals metal. Both EOPE and SHG show significant values at smaller applied frequencies, and their values slightly decrease at higher dispersion frequency (1064 nm).

The calculated frequency-dependent second hyperpolarizability $\gamma(\omega)$ that includes dc-Kerr $\gamma^{\text{dc-Kerr}}(\omega) = \gamma(-\omega;\omega,0,0)$ and second harmonic generation with $\gamma^{\text{EFSHG}}(\omega) = \gamma(-2\omega;\omega,\omega,0)$ are calculated at the same level of theory. The calculated values of dynamic second hyperpolarizability are

Table 5 Frequency-dependent hyperpolarizability $\beta(\omega)$ in form of electro-optic pockel's effect (EOPE) $\beta(-\omega;\omega,0)$ in $\times 10^{-33}$ esu, and electric field induced second harmonic generation (EFSHG) with $\beta(2-\omega;\omega,\omega)$ in $\times 10^{-33}$ esu at $\omega = 532$ nm and $\omega = 1064$ nm

	$\omega = 0.0856$ au (532 nm)		$\omega = 0.0428$ au (1064 nm)	
	$\beta(-\omega;\omega,0)$	$\beta(-2\omega;\omega,0)$	$\beta(-\omega;\omega,0)$	$\beta(-2\omega;\omega,0)$
Ge_5AM_3				
Ge_5Li_3 (A)	3.28×10^{-27}	4.42×10^{-27}	6.99×10^{-29}	1.81×10^{-28}
Ge_5Na_3 (B)	1.29×10^{-27}	3.63×10^{-27}	2.50×10^{-28}	3.72×10^{-28}
Ge_5K_3 (C)	3.54×10^{-26}	1.30×10^{-26}	2.24×10^{-28}	9.50×10^{-28}
Ge_9AM_5				
Ge_9Li_5 (D)	3.02×10^{-29}	3.28×10^{-29}	7.86×10^{-29}	1.47×10^{-30}
Ge_9Na_5 (E)	7.68×10^{-28}	4.42×10^{-27}	1.56×10^{-26}	2.94×10^{-27}
Ge_9K_5 (F)	6.39×10^{-27}	1.04×10^{-26}	4.93×10^{-29}	1.39×10^{-27}
$\text{Ge}_{10}\text{AM}_3$				
$\text{Ge}_{10}\text{Li}_3$ (G)	9.67×10^{-29}	1.98×10^{-28}	2.24×10^{-29}	6.99×10^{-29}
$\text{Ge}_{10}\text{Na}_3$ (H)	5.71×10^{-28}	3.71×10^{-28}	2.85×10^{-29}	5.62×10^{-29}
Ge_{10}K_3 (I)	1.21×10^{-27}	1.04×10^{-27}	5.87×10^{-29}	2.42×10^{-28}

Table 6 Frequency-dependent second hyperpolarizability with dc-Kerr effect $\gamma(-\omega; \omega, 0, 0)$ and electric field induced second harmonic generation (ESHG) $\gamma(-2\omega; \omega, \omega, 0)$ in $\times 10^{-40}$ esu at $\omega = 532$ and 1064 nm

Superalkalis	$\omega = 0.0856$ au (532 nm)		$\omega = 0.0428$ au (1064 nm)	
	$\gamma(-\omega; \omega, 0, 0)$	$\gamma(-2\omega; \omega, \omega, 0)$	$\gamma(-\omega; \omega, 0, 0)$	$\gamma(-2\omega; \omega, \omega, 0)$
Ge₅AM₃				
Ge ₅ Li ₃ (A)	7.84×10^{-31}	1.37×10^{-30}	3.39×10^{-34}	1.40×10^{-30}
Ge ₅ Na ₃ (B)	1.30×10^{-32}	1.64×10^{-31}	2.45×10^{-33}	2.31×10^{-33}
Ge ₅ K ₃ (C)	5.43×10^{-36}	2.52×10^{-29}	7.37×10^{-32}	2.09×10^{-31}
Ge₉AM₅				
Ge ₉ Li ₅ (D)	1.36×10^{-33}	5.74×10^{-32}	3.16×10^{-32}	1.19×10^{-33}
Ge ₉ Na ₅ (E)	1.76×10^{-29}	8.80×10^{-30}	1.58×10^{-31}	1.03×10^{-32}
Ge ₉ K ₅ (F)	5.23×10^{-32}	2.53×10^{-32}	2.15×10^{-30}	$3.76 \ 747 \ 508 \times 10^{-32}$
Ge₁₀AM₃				
Ge ₁₀ Li ₃ (G)	8.45×10^{-32}	1.24×10^{-31}	3.24×10^{-40}	5.28×10^{-34}
Ge ₁₀ Na ₃ (H)	1.22×10^{-32}	6.84×10^{-34}	1.72×10^{-32}	2.41×10^{-33}
Ge ₁₀ K ₃ (I)	5.23×10^{-32}	2.53×10^{-32}	2.15×10^{-30}	3.76×10^{-32}

given in Table 6. The calculated dc-Kerr constant and EFSHG are higher at 532 nm and their values slightly decreased at higher dispersion frequency (1064 nm). Likewise, Ge₉AM₅ and Ge₁₀AM₃ are also larger at a small dispersion frequency of 532 nm. Hence, the studied clusters offer tremendous dynamic NLO properties at the smaller external applied frequency.

4 Conclusion

In the summary, we explored the zintl-based superalkali for geometric, electronic and nonlinear optical properties. The studied zintl superalkali clusters Ge₅AM₃, Ge₉AM₅, and Ge₁₀AM₃ (AM = Li, Na, K) belong to excess electron compounds. These are superalkali clusters as their calculated vertical ionization potential (VIP) values are smaller than Li atom (5.39 eV). The calculated significant VIP values suggest their electronic stability. The calculated chemical hardness (η) lie in the range of 2.13 to 4.51 eV, and Ge₉AM₅ shows the higher softness among the series. There is a significant charge (positive in magnitude) on alkali metals, and the charge is transferred from alkali to Ge-atom. The charge is transferred from alkali metals to Ge-atoms within the clusters. There is a notable reduction in E_{H-L} (0.79–4.04 eV) which reveals their conductive applications. These clusters are completely transparent in the deep UV region, and show absorption maxima (λ_{max}) at the longer wavelength. Being excess electron compounds these clusters shows remarkable hyperpolarizability response up to 8.99×10^{-26} esu where the static second hyperpolarizability (γ_0) value recorded up to 2.15×10^{-30} esu for Ge₉AM₅ clusters. The adopted two-level model study reveals the controlling factors of hyperpolarizability. The obtained significant β_{tl} value of 1.90×10^{-27} esu may attributed to smaller excitation energy (0.01 eV) The frequency-dependent hyperpolarizabilities and second hyperpolarizabilities values are much higher at smaller dispersion frequencies ($\omega = 532$ nm). Moreover, the hyper Rayleigh scattering (β_{HRS}) increases up to 5.03×10^{-27} esu for the Ge₉K₅ cluster.

Conflicts of interest

There are no conflicts to declare.

Acknowledgements

The authors acknowledge the financial and technical support from the Higher Education Commission of Pakistan and COMSATS University, Abbottabad Campus.

References

- 1 C. Chen and G. Liu, Recent advances in nonlinear optical and electro-optical materials, *Annu. Rev. Mater. Sci.*, 1986, **16**(1), 203–243.
- 2 S. J. Qin and T. A. Badgwell, An overview of nonlinear model predictive control applications, in *Nonlinear model predictive control*, Springer, 2000, pp. 369–392.
- 3 T. H. Maiman, Stimulated optical radiation in ruby, *Nature*, 1960, **187**(4736), 493–494.
- 4 V. M. Agranovich, Y. N. Gartstein and M. Litinskaya, Hybrid resonant organic-inorganic nanostructures for optoelectronic applications, *Chem. Rev.*, 2011, **111**(9), 5179–5214.
- 5 J. Guo, *et al.*, 2D GeP as a novel broadband nonlinear optical material for ultrafast photonics, *Laser Photon. Rev.*, 2019, **13**(9), 1900123.
- 6 H. Yu, N. Z. Koocher, J. M. Rondinelli and P. S. Halasyamani, Pb₂BO₃I: A Borate Iodide with the Largest Second-Harmonic Generation (SHG) Response in the KBe₂BO₃F₂ (KBBF) Family of Nonlinear Optical (NLO) Materials, *Angew. Chem. Int. Ed.*, 2018, **57**(21), 6100–6103.
- 7 A. Lukic, *et al.*, Endoscopic fiber probe for nonlinear spectroscopic imaging, *Optica*, 2017, **4**(5), 496–501.
- 8 B. Wang, I. Riemann, H. Schubert, D. Schweitzer, K. König and K. Halbhüter, Multiphoton microscopy for monitoring



intratissue femtosecond laser surgery effects, *Lasers Surg. Med.*, 2007, **39**(6), 527–533.

9 M. Nakano, *et al.*, Second Hyperpolarizabilities (γ) of Bisimidazole and Bistriazole Benzenes: Diradical Character, Charged State, and Spin State Dependences, *J. Phys. Chem. A*, 2006, **110**, 4238.

10 Y.-K. Lee, S.-J. Jeon and M. Cho, Molecular polarizability and first hyperpolarizability of octupolar molecules: donor-substituted triphenylmethane dyes, *J. Am. Chem. Soc.*, 1998, **120**(42), 10921–10927.

11 L. Karki, F. W. Vance, J. T. Hupp, S. M. LeCours and M. J. Therien, Electronic Stark Effect Studies of a Porphyrin-Based Push–Pull Chromophore Displaying a Large First Hyperpolarizability: State-Specific Contributions to β , *J. Am. Chem. Soc.*, 1998, **120**(11), 2606–2611.

12 S.-J. Wang, Y.-F. Wang and C. Cai, Multidecker Sandwich Complexes $VnBenn+1$ ($n = 1, 2, 3$) as Stronger Electron Donor Relative to Ferrocene for Designing High-Performance Organometallic Second-Order NLO Chromophores: Evident Layer Effect on the First Hyperpolarizability and Two-Dimensional N, *J. Phys. Chem. C*, 2015, **119**, 5589.

13 R. L. Zhong, H. L. Xu, Z. R. Li and Z. M. Su, Role of excess electrons in nonlinear optical response, *J. Phys. Chem. Lett.*, 2015, **6**(4), 612–619.

14 P. S. Halasyamani and W. Zhang, *inorganic materials for UV and deep-UV nonlinear-optical applications*, ACS Publications, 2017.

15 X.-H. Li, L. Zhang, X.-L. Zhang, B.-L. Ni, C.-Y. Li and W.-M. Sun, Designing a new class of excess electron compounds with unique electronic structures and extremely large nonlinear optical responses, *New J. Chem.*, 2020, **44**, 6411–6419.

16 H. M. He, *et al.*, Effects of the Cage Number and Excess Electron Number on the Second Order Nonlinear Optical Response in Molecular All-Metal Electride Multicage Chains, *J. Phys. Chem. C*, 2017, **121**(45), 25531–25540.

17 F. Ma, *et al.*, Lithium salt electride with an excess electron pair – A class of nonlinear optical molecules for extraordinary first hyperpolarizability, *J. Phys. Chem. A*, 2008, **112**(45), 11462–11467.

18 W. M. Sun, *et al.*, Designing Alkalides with Considerable Nonlinear Optical Responses and High Stability Based on the Facially Polarized Janus all-cis-1,2,3,4,5,6-Hexafluorocyclohexane, *Organometallics*, 2017, **36**(17), 3352–3359.

19 A. Ahsan and K. Ayub, Adamanzane based alkaline earthides with excellent nonlinear optical response and ultraviolet transparency, *Opt. Laser Technol.*, 2020, **129**, 106298.

20 A. K. Srivastava and N. Misra, $M2X$ ($M = Li, Na; X = F, Cl$): the smallest superalkali clusters with significant NLO responses and electride characteristics, *Mol. Simul.*, 2016, **42**(12), 981–985.

21 J. L. Dye, Electrides: Early Examples of Quantum Confinement, *Acc. Chem. Res.*, 2009, **42**(10), 1564–1572.

22 R. H. Huang, J. L. Eglin, S. Z. Huang, L. E. H. McMills and J. L. Dye, Complexation of the cations of six alkalides and an electride by mixed crown ethers, *J. Am. Chem. Soc.*, Oct. 1993, **115**(21), 9542–9546.

23 A. Ahsan and K. Ayub, Extremely large nonlinear optical response and excellent electronic stability of true alkaline earthides based on hexaammine complexant, *J. Mol. Liq.*, 2020, **297**, 111899.

24 F. Ullah, N. Kosar, K. Ayub and T. Mahmood, Superalkalis as a source of diffuse excess electrons in newly designed inorganic electrides with remarkable nonlinear response and deep ultraviolet transparency: A DFT study, *Appl. Surf. Sci.*, 2019, **483**, 1118–1128.

25 J. Iqbal, R. Ludwig and K. Ayub, Phosphides or nitrides for better NLO properties? A detailed comparative study of alkali metal doped nano-cages, *Mater. Res. Bull.*, 2017, **92**, 113–122.

26 F. Ullah, N. Kosar, A. Ali, T. Mahmood and K. Ayub, Alkaline earth metal decorated phosphide nanoclusters for potential applications as high performance NLO materials; A first principle study, *Phys. E*, 2020, **118**, 113906.

27 A. S. Rad and K. Ayub, Nonlinear optical and electronic properties of Cr-, Ni-, and Ti-substituted C₂₀ fullerenes: a quantum-chemical study, *Mater. Res. Bull.*, 2018, **97**, 399–404.

28 A. S. Rad and K. Ayub, Substitutional doping of zirconium-, molybdenum-, ruthenium-, and palladium: An effective method to improve nonlinear optical and electronic property of C₂₀ fullerene, *Comput. Theor. Chem.*, 2017, **1121**, 68–75.

29 N. Kosar, K. Shehzadi, K. Ayub and T. Mahmood, Theoretical study on novel superalkali doped graphdiyne complexes: Unique approach for the enhancement of electronic and nonlinear optical response, *J. Mol. Graphics Modell.*, 2020, 107573.

30 H. Sajid, K. Ayub and T. Mahmood, Exceptionally high NLO response and deep ultraviolet transparency of superalkali doped macrocyclic oligofuran rings, *New J. Chem.*, 2020, **44**(6), 2609–2618.

31 B. G. A. Brito, G.-Q. Hai and L. Cândido, Analysis of the ionization potentials of small superalkali lithium clusters based on quantum Monte Carlo simulations, *Chem. Phys. Lett.*, 2018, **708**, 54–60.

32 E. Cochran, G. Muller and G. Meloni, Stability and bonding of new superalkali phosphide species, *Dalton Trans.*, 2015, **44**(33), 14753–14762.

33 T. Zhao, Q. Wang and P. Jena, Rational design of superalkalis and their role in CO₂ activation, *Nanoscale*, 2017, **9**(15), 4891–4897.

34 N. Hou, Y.-Y. Wu, H.-S. Wu and H.-M. He, The important role of superalkalis on the static first hyperpolarizabilities of new electrides: Theoretical investigation on superalkali-doped hexamethylenetetramine (HMT), *Synth. Met.*, 2017, **232**, 39–45.

35 W.-M. Sun, *et al.*, A theoretical study on superalkali-doped nanocages: unique inorganic electrides with high stability, deep-ultraviolet transparency, and a considerable



nonlinear optical response, *Dalton Trans.*, 2016, **45**(17), 7500–7509.

36 K. Shehzadi, K. Ayub and T. Mahmood, Theoretical study on design of novel superalkalis doped graphdiyne: A new donor-acceptor (D- π -A) strategy for enhancing NLO response, *Appl. Surf. Sci.*, 2019, **492**, 255–263.

37 W. M. Sun, L. T. Fan, Y. Li, J. Y. Liu, D. Wu and Z. R. Li, On the potential application of superalkali clusters in designing novel alkalides with large nonlinear optical properties, *Inorg. Chem.*, 2014, **53**(12), 6170–6178.

38 J. J. Wang, *et al.*, The interaction between superalkalis (M 3 O, M = Na, K) and a C 20 F 20 cage forming superalkali electride salt molecules with excess electrons inside the C 20 F 20 cage: Dramatic superalkali effect on the nonlinear optical property, *J. Mater. Chem.*, 2012, **22**(19), 9652–9657.

39 A. K. Srivastava and N. Misra, Nonlinear optical behavior of LinF (n = 2–5) superalkali clusters, *J. Mol. Model.*, 2015, **21**(12), 1–5.

40 D. Hou, D. Wu, W. M. Sun, Y. Li and Z. R. Li, Evolution of structure, stability, and nonlinear optical properties of the heterodinuclear CNLin (n = 1–10) clusters, *J. Mol. Graphics Modell.*, 2015, **59**, 92–99.

41 M. J. T. Oliveira, P. V. C. Medeiros, J. R. F. Sousa, F. Nogueira and G. K. Gueorguiev, Optical and magnetic excitations of metal-encapsulating Si cages: A systematic study by time-dependent density functional theory, *J. Phys. Chem. C*, 2014, **118**(21), 11377–11384.

42 M. I. A. Oliveira, R. Rivelino, F. de Brito Mota and G. K. Gueorguiev, Optical properties and quasiparticle band gaps of transition-metal atoms encapsulated by silicon cages, *J. Phys. Chem. C*, 2014, **118**(10), 5501–5509.

43 S. Scharfe, F. Kraus, S. Stegmaier, A. Schier and T. F. Fässler, Zintl ions, cage compounds, and intermetallic clusters of group 14 and group 15 elements, *Angew. Chem. Int. Ed.*, 2011, **50**(16), 3630–3670.

44 S. Giri, G. N. Reddy and P. Jena, Organo-Zintl Clusters [P7R4]: A New Class of Superalkalis, *J. Phys. Chem. Lett.*, 2016, **7**(5), 800–805.

45 G. N. Reddy, A. V. Kumar, R. Parida, A. Chakraborty and S. Giri, Zintl superalkalis as building blocks of supersalts, *J. Mol. Model.*, 2018, **24**(11), 1–13.

46 W. Sun, Decorating Zintl polyanions with alkali metal cations: A novel strategy to design superatom cations with low electron affinity, *J. Alloys Compd.*, 2018, **740**, 400–405.

47 M. J. Frischet *et al.*, *Gaussian 09 (Revision A. 02)[Computer software]*, Gaussian Inc., Wallingford CT, 2009.

48 T. Yanai, D. P. Tew and N. C. Handy, A new hybrid exchange-correlation functional using the Coulomb-attenuating method (CAM-B3LYP), *Chem. Phys. Lett.*, 2004, **393**(1–3), 51–57.

49 M. T. P. Beerepoot, D. H. Friese, N. H. List, J. Kongsted and K. Ruud, Benchmarking two-photon absorption cross sections: performance of CC2 and CAM-B3LYP, *Phys. Chem. Chem. Phys.*, 2015, **17**(29), 19306–19314.

50 M. Li, J. R. Reimers, M. J. Ford, R. Kobayashi and R. D. Amos, Accurate prediction of the properties of materials using the CAM-B3LYP density functional, *J. Comput. Chem.*, 2021, **1486**–1497.

51 P. A. Limacher, K. V. Mikkelsen and H. P. Luthi, On the Accurate Calculation of Polarizabilities and Second Hyperpolarizabilities of Polyacetylene Oligomer Chains using the CAM-B3LYP Density Functional, *J. Chem. Phys.*, 2009, **130**, 194114.

52 A. Ahsin and K. Ayub, Remarkable electronic and NLO properties of bimetallic superalkali clusters: a DFT study, *J. Nanostruct. Chem.*, 2021, 1–17.

53 M. B. Oviedo, N. V. Ilawe and B. M. Wong, Polarizabilities of π -conjugated chains revisited: improved results from broken-symmetry range-separated DFT and new CCSD (T) benchmarks, *J. Chem. Theory Comput.*, 2016, **12**(8), 3593–3602.

54 R. Vijayaraj, V. Subramanian and P. K. Chattaraj, Comparison of Global Reactivity Descriptors Calculated Using Various Density Functionals: A QSAR Perspective, *J. Chem. Theory Comput.*, Oct. 2009, **5**(10), 2744–2753.

55 S. K. Pathak, *et al.*, Experimental (FT-IR, FT-Raman, UV and NMR) and quantum chemical studies on molecular structure, spectroscopic analysis, NLO, NBO and reactivity descriptors of 3,5-Difluoroaniline, *Spectrochim. Acta, Part A*, 2015, **135**, 283–295.

56 A. Ahsin, A. Ali and K. Ayub, Alkaline earth metals serving as source of excess electron for alkaline earth metals to impart large second and third order nonlinear optical response; A DFT study, *J. Mol. Graphics Modell.*, 2020, **101**, 107759.

57 F. Ullah, N. Kosar, K. Ayub, M. A. Gilani and T. Mahmood, Theoretical study on a boron phosphide nanocage doped with superalkalis: novel electrides having significant nonlinear optical response, *New J. Chem.*, 2019, **43**(15), 5727–5736.

58 N. Kosar, *et al.*, Significant nonlinear optical response of alkaline earth metals doped beryllium and magnesium oxide nanocages, *Mater. Chem. Phys.*, 2020, **242**, 122507.

59 A. S. Rad and K. Ayub, Change in the electronic and nonlinear optical properties of Fullerene through its incorporation with Sc-, Fe-, Cu-, and Zn transition metals, *Appl. Phys. A*, 2019, **125**(6), 430.

60 S. Sajjad, A. Ali, T. Mahmood and K. Ayub, Journal of Molecular Graphics and Modelling Janus alkaline earthides with excellent NLO response from sodium and potassium as source of excess electrons ; a first principles study, *J. Mol. Graphics Modell.*, 2020, **100**, 107668.

61 F. Ullah, K. Ayub and T. Mahmood, Remarkable second and third order nonlinear optical properties of organometallic C₆Li₆–M₃O electrides, *New J. Chem.*, 2020, **44**, 9822–9829.

62 K. Ayub, Are phosphide nano-cages better than nitride nano-cages? A kinetic, thermodynamic and non-linear optical properties study of alkali metal encapsulated X₁₂Y₁₂ nano-cages, *J. Mater. Chem. C*, 2016, **4**(46), 10919–10934.



63 S. Munsif, *et al.*, Remarkable nonlinear optical response of alkali metal doped aluminum phosphide and boron phosphide nanoclusters, *J. Mol. Liq.*, 2018, **271**, 51–64.

64 A. Ahsin and K. Ayub, Theoretical Investigation of Superalkali Clusters M₂OCN and M₂NCO (where M= Li, Na, K) as Excess Electron System with Significant Static and Dynamic Nonlinear optical response, *Opt.*, 2020, 166037.

65 A. Ahsin and K. Ayub, Superalkali-based alkalides Li₃O@[12-crown-4]M (where M= Li, Na, and K) with remarkable static and dynamic NLO properties; A DFT study, *Mater. Sci. Semicond. Process.*, 2022, **138**, 106254.

